J Nanopart Res (2015) 17:130
DOI 10.1007/s11051-015-2946-0

RESEARCH PAPER

Tailoring the chemical composition and dispersion behavior of fluorinated graphene oxide via CF_4 plasma

Baoming Zhou · Xiaoming Qian · Mingming Li · Jilan Ma · Liangsen Liu · Chuansheng Hu · Zhiwei Xu · Xiaoning Jiao

Received: 16 December 2014 / Accepted: 3 March 2015 / Published online: 10 March 2015

Abstract Grafting fluorine onto graphene oxide (GO) by CF_4 plasma treatment was investigated in this study. An easy, low-cost, and effective synthesis of the high-dispersive fluorinated GO (FGO) with tunable atomic ratio of F/O ($R_{F/O}$) has been realized and the $R_{F/O}$ can be readily manipulated just by adjusting the reaction time. The influence of plasma treatment time on the microstructure, morphology, and dispersion of graphene nanosheets was systematically analyzed. X-ray photoelectron spectroscopy analysis confirmed that fluorine has been grafted onto graphene, and the $R_{F/O}$ was gradually increased to 3.54 for the FGO treated for 20 min. Morphology investigation indicated that etching on the edge of GO occurred during the fluorination. The dispersion performance of FGO in water reduced continuously, which in *N*,*N*-dimethylacetamide (DMAc) increased firstly and then decreased with the increase in plasma time. The zeta potentials of FGO in DMAc reached the lowest at −28.6 mV when GO was treated for 10 min. The dispersion of FGO in water should be attributed to the decrease of C–O group, while there was a same variation trend of FGO zeta potential in DMAc as the value of C–F content, regardless of $R_{F/O}$, CF_2 group content and CF_3 group content. The GO film was super-hydrophilic and the film of FGO treated for 20 min was found to be neither hydrophilic nor hydrophobic.

Keywords Plasma · Fluorinated graphene oxide · Fluorine-containing groups · Dispersion · Synthesis

B. Zhou · X. Qian · M. Li · J. Ma · L. Liu (✉) · C. Hu · Z. Xu · X. Jiao
Key Laboratory of Advanced Braided Composites, Ministry of Education, School of Textiles, Tianjin Polytechnic University, Tianjin 300387, People's Republic of China
e-mail: 83019163@163.com

Introduction

The achievement of mechanical exfoliation of single-layer graphene in 2004 (Novoselov et al. 2004), as a one-atom-thick sheet of sp^2-bonded hexagonal carbon atom lattice (Geim and Novoselov 2007; Meyer et al. 2007), initiated a rush on the exploitation of this fascinating nanomaterial with exceptional mechanical (Lee et al. 2008), chemical (Dreyer et al. 2010; Stankovich et al. 2006), thermal (Balandin et al. 2008), and electrical (Zhang et al. 2005) properties. Although pristine graphene has been endowed with unparalleled properties, it was also reported that pristine graphene was hydrophobic and has very limited solubility in most of the solvents. To impart solution processability of graphene, the most important way was to functionalize this two-dimensional insoluble material (Loh et al. 2010). Unfortunately, it was difficult to directly and chemically functionalize graphene because of the hydrophobic and chemically inert nature of pristine graphene. Thus, attempts to overcome this issue have

mainly focused on functionalization of graphene oxide (GO) due to its more chemical reaction than graphene (Ai et al. 2013).

GO was heavily oxygenated, bearing hydroxyl, epoxy, and carboxylic groups on their basal planes, making it strongly hydrophilic, which allowed its dispersion and swelling in water (Dreyer et al. 2010). However, the strong tendency of graphene layers to stack between each other because of van der Waals interactions prevents their solubilization in any medium (Stankovich et al. 2006). Therefore, a critical aspect in the graphene manipulation was to prevent the restacking of graphene sheets. So far, chemical functionalization of graphene has focused on improving its solubility/processability in both water and organic solvents using different soluble groups (Eda et al. 2008; Si and Samulski 2008). Fluorine was one candidate to provide more stable graphene derivatives with stronger binding between agents and carbon, such as the fluorination of bulk graphite (Palin and Wadsworth 1948), carbon nanotubes (Plank et al. 2003), and graphene sheets (Bon et al. 2009). Fluorinated graphene was either a high-quality insulator with high Young's modulus (Nair et al. 2010), or an effective p-type doped semiconductor with high thermal and chemical stability (Wang et al. 2012). It was also a favorable biomaterial for treating cancer and promoting neuro-induction of stem cells (Romero-Aburto et al. 2013). Yet a prerequisite for realization of these brilliant performances was that fluorinated graphene sheets can be readily prepared. So a reliable and easy method for producing fluorinated graphene sheets was of particular significance to fully display fluorinated graphene's properties and explore its potential applications.

At present, the experimental synthesis of fluorinated graphene, which has been cited in a few reports, could be divided into two systems: (1) directly fluorinating graphene sheets utilizing XeF_2 (Stine et al. 2013) or F_2 (Matsutani et al. 2013) and hydrogen fluoride by thermal (Wang et al. 2012), electrochemical(Bruna et al. 2011), and photochemical (Gong et al. 2013) routes, and (2) exfoliating graphite fluoride (Zbořil et al. 2010; Zhang et al. 2013) by mechanical cleavage or ultrasonication in sulfolane, isopropanol, or ionic liquid. However, intrinsic disadvantages were inevitable in these systems. The use of XeF_2 requires high thermal treatment temperature (>350 °C) during the fluorination process, which can result in inevitable aggregation. Yet HF is also toxic and highly corrosive. Moreover, the XeF_2 and graphite fluoride are too expensive to be generalized, especially for XeF_2. Under such circumstances, plasma treatment (Bon et al. 2009; Yue et al. 2015) is considered to be one of the tricks to overcome the difficulties. Recently, plasma-based functionalization has been reported which is a gas-phase functionalization technique to change the electronic structure of graphene such as doping and band gap opening, and it provides the possibility of the reaction between graphene and fluorinating agents (Chen et al. 2012; Shen et al. 2012). This kind of functionalization technique provides a convenient method of fluoridizing graphene in aneroid environment.

Drawn by this idea, the plasma-assisted gas-phase decomposition method was designed for the fluorination treatment of GO at room temperature via CF_4. The purpose of this paper was to obtain the fluorinated GO (FGO) with different fluorine/oxygen ratios ($R_{F/O}$) and fluorine-containing groups as a function of treatment time, and to investigate the effect of functional groups on dispersion behavior. The chemical composition, morphology, fluorination mechanism, and dispersion performance of FGO were investigated and discussed. X-ray photoelectron spectroscopy (XPS) was used to estimate the influence of treatment time on the surface chemical contents of graphene nanosheets. X-ray diffraction (XRD) was used to reveal the influence of fluorination on the interlayer structure of GO. The surface morphology and structural changes of graphene before and after fluorination were found by atomic force microscopy (AFM) and transmission electron microscopy (TEM). For further study, the hydrophilicity and the dispersion in aqueous solution or organic solution of FGO were observed by water contact-angle and zeta potential measurements. Along with various $R_{F/O}$ values, the FGO samples present different dispersions. The useful experimental results and interesting achievements presented here are expected to promote FGO to find more applications in various fields and cast enlightening light on graphene modification.

Experimental

Materials

Graphite was purchased from the Qingdao Ruisheng Graphite Co. Ltd., China. H_3PO_4, $KMnO_4$ with analytical grade and 98 % H_2SO_4, 30 % H_2O_2 aqueous

solution, *N*,*N*-dimethylacetamide (DMAc, >99.5 %, reagent) and other common chemicals were purchased from Tianjin Weichen Chemical Reagent Co. Ltd., China.

Preparation of GO

Graphite oxide was prepared by an improved Hummers' method (Shi et al. 2012). Briefly, a 9:1 mixture of concentrated H_2SO_4/H_3PO_4 (360:40 ml) was added to a mixture of 3.0 g graphite flakes and 18.0 g $KMnO_4$, producing a slight exotherm to 35–40 °C. The reaction was then heated to 50 °C and stirred for 12 h. The reactants were cooled to room temperature and poured onto ice (~400 ml). The mixture was centrifuged and the supernatant was decanted away. The remaining solid material (graphite oxide) was rinsed repeatedly in deionized water until the pH of the solution reached approximately 7.0. It was dried by a freeze-drying method and then dispersed into distilled water. The suspended GO sheets were obtained after 3 h of ultrasonic treatment. The suspension (2 mg/ml) was poured into Petri dishes (90 mm in diameter). The samples were allowed to freeze for more than 4 h, at which point linear ice crystals extending throughout the polymer could be seen. The solidified gelatin/water systems were then transferred into a freeze-drying vessel under vacuum (<20 Pa) and freeze-dried for 48 h (Wu et al. 2010), and another 48 h under vacuum at room temperature was required to remove the residual water. Finally, GO was obtained.

Fluorination of GO

To form FGO, the microwave plasma etcher (YZ-Z) was employed to finish the process of fluorination at room temperature with the CF_4 flow. The chamber was evacuated at 5 Pa and the temperature was set to room temperature. After the CF_4 gas was inlet into the chamber, the gas flow and pressure was controlled. The degree of fluorination process was adjusted by controlling the exposure time when the plasma was ignited. The CF_4 plasma treatment conditions for GO were as follows: gas flow rate of 1.5 l/h, operating pressure of 20 Pa, a bias of 200 V, the power of 240 W, and process duration of 1, 3, 5, 10, 15, 20 min, respectively, and these graphene nanosheets were named as FGO-1, FGO-3, FGO-5, FGO-10, FGO-15, and FGO-20, correspondingly.

Characterization of FGO

The elementary analysis was performed by XPS (Thermo ESCALAB 250). The morphology and thickness of different sheet-like samples were observed by AFM (CSPM5500) under the tapping mode. XRD with Cu Kα radiation ($\gamma = 1.5418$ Å) was used to reveal the influence of fluorination on the interlayer structure of GO. TEM and high-resolution TEM (HRTEM, FEI Tecnai F30, operated at 300 kV) were also employed to investigate the microstructure and morphology of the samples. The optical absorption of the samples was measured by an ultraviolet–visible (UV–Vis) spectrophotometer (UV-1800). Zeta potential of FGO (1 mg/ml) in water and DMAc were determined using a Delsa Nano C analyzer and all data were measured over five times. All the samples were dispersed by ultrasonic agitation at 298.15 K for 1 h before tests.

Contact-angle measurements of FGO film

The contact angle between water and the FGO film was measured with contact-angle measurement apparatus (JYSP-180 contact angle analyzer) based on the sessile-drop method. Briefly, 2.5 mg/ml FGO aqueous suspension was formed, and then 3 ml suspension was spread onto a clean microscope slide. After being wetted with the suspension, the FGO-covered slide was dried at room temperature and then 50 °C for 12 h until a dried thin film was formed. A water droplet was deposited on a flat homogeneous graphene film surface and the contact angle of the droplet with the surface was measured. The instantaneous contact angle obtained within 0.2 s (ensuring observable vibration of the liquid drop on the solid sample had already eased) was recorded. Each contact angle was measured five times at five different points of each film sample and an average value was calculated.

Results and discussion

XPS analysis of fluorinated and pristine GO

Figure 1 shows the XPS survey spectra of the GO and FGO-10 recorded. The peaks at 284.6 and 532.8 eV, observed on two spectra, were attributed to C1s and O1s, respectively (Gong et al. 2014). On the XPS spectrum of FGO-10 recorded, a peak near 688 eV can

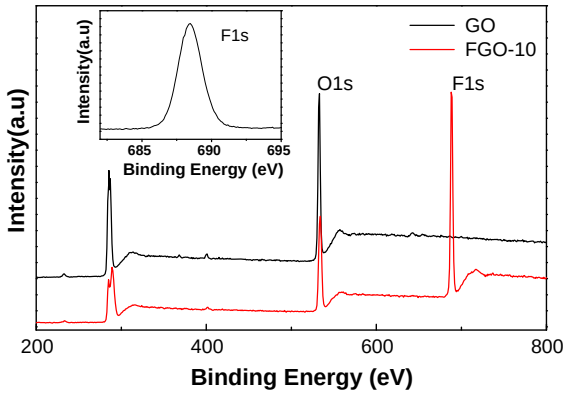

Fig. 1 XPS survey spectra recorded on GO and FGO-10, and F1s spectra of FGO-10 shown in the *inset*

be observed. This peak was generated by photoelectrons emitted from F1s core level, suggesting an effective grafting of fluorine on the GO surface (Gong et al. 2014; Xu et al. 2007).

The grafting efficiency was affected by the treatment time. The measured carbon, fluorine, and oxygen atomic concentrations are shown in Fig. 2. Within the treatment time investigated, the fluorine concentration in FGO was found to increase with treatment time. At the beginning (1 min), the atomic fluorine concentration was quite low and about 9.09 %. With increase in time, the concentration of F1s increased and the concentration of C1s and O1s decreased (Wang et al. 2013). The method of topotactic synthesis gave rise to very high level of fluorination. For instance, the molar ratio of F/C ($R_{F/C}$) observed was 0.96, and the values of F/O molar ratio ($R_{F/O}$) observed was as high as 3.54 for FGO-20. Even if the treatment time was only 1 min, the F/C ratio achieves at 0.14. The $R_{F/C}$ and $R_{F/O}$ can be easily adjusted by controlling the reaction conditions (Wang et al. 2012). During a plasma treatment, the excited species, radicals, electrons, ions, and UV light could interact with the surface of the GO, breaking C–C/C–O bonds and creating active sites for bonding of functional groups. For a longer treatment time, the etching phenomenon will occur and remove the surface atoms along with the functionalized groups.

Corresponding C1s peaks of XPS spectra are also shown in Fig. 3, and assignments are listed in Table 1. The C1s spectrum of GO can be fitted into three peaks centered at about 284.7, 287.3, and 288.7 eV, corresponding to C–C, –C–O, and –COOH groups (Gong et al. 2014), respectively. The fluorination degree of FGO can be recognized by estimating the relative content of F–C from high-resolution C1s spectra by the sum of the F content in each group. The C1s curve fit spectrum of FGO-1 exhibited the component corresponding to groups C–F bonds, which was assigned at 290.5 eV (Wang et al. 2013). The intensity of peak (C–F) component increased obviously with plasma time at the beginning, while showed a sharp decrease later. This decrease may have resulted from the reduction of the conjugated π domains. Meanwhile, the share of CF_2 and CF_3 components had some increases. CF_2 and CF_3 bonds were generated because of the vacancy defects in GO at high plasma power and long time and C–F bond was produced after a short fluorination time. Thus, the raising degree of

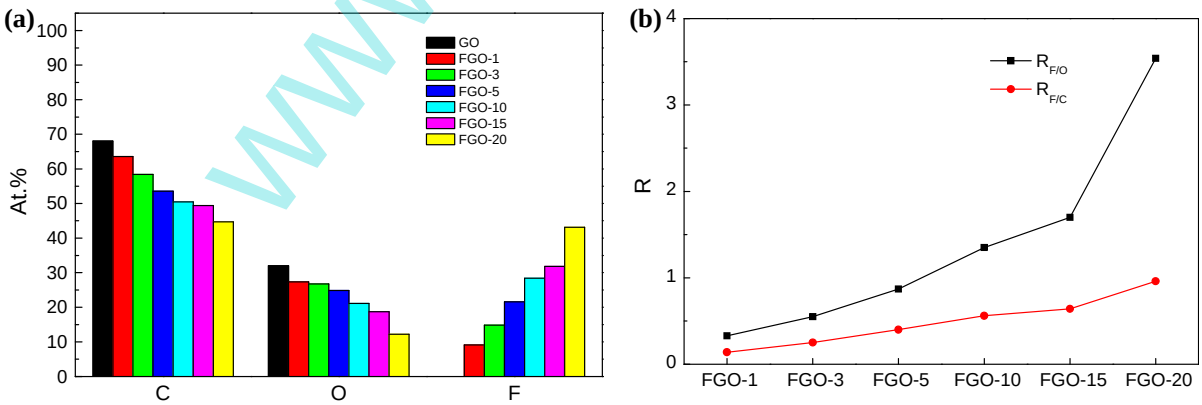

Fig. 2 The carbon, fluorine, and oxygen atomic concentrations of fluorinated and pristine GO (**a**) and the atomic ratio of F/O and F/C (**b**)

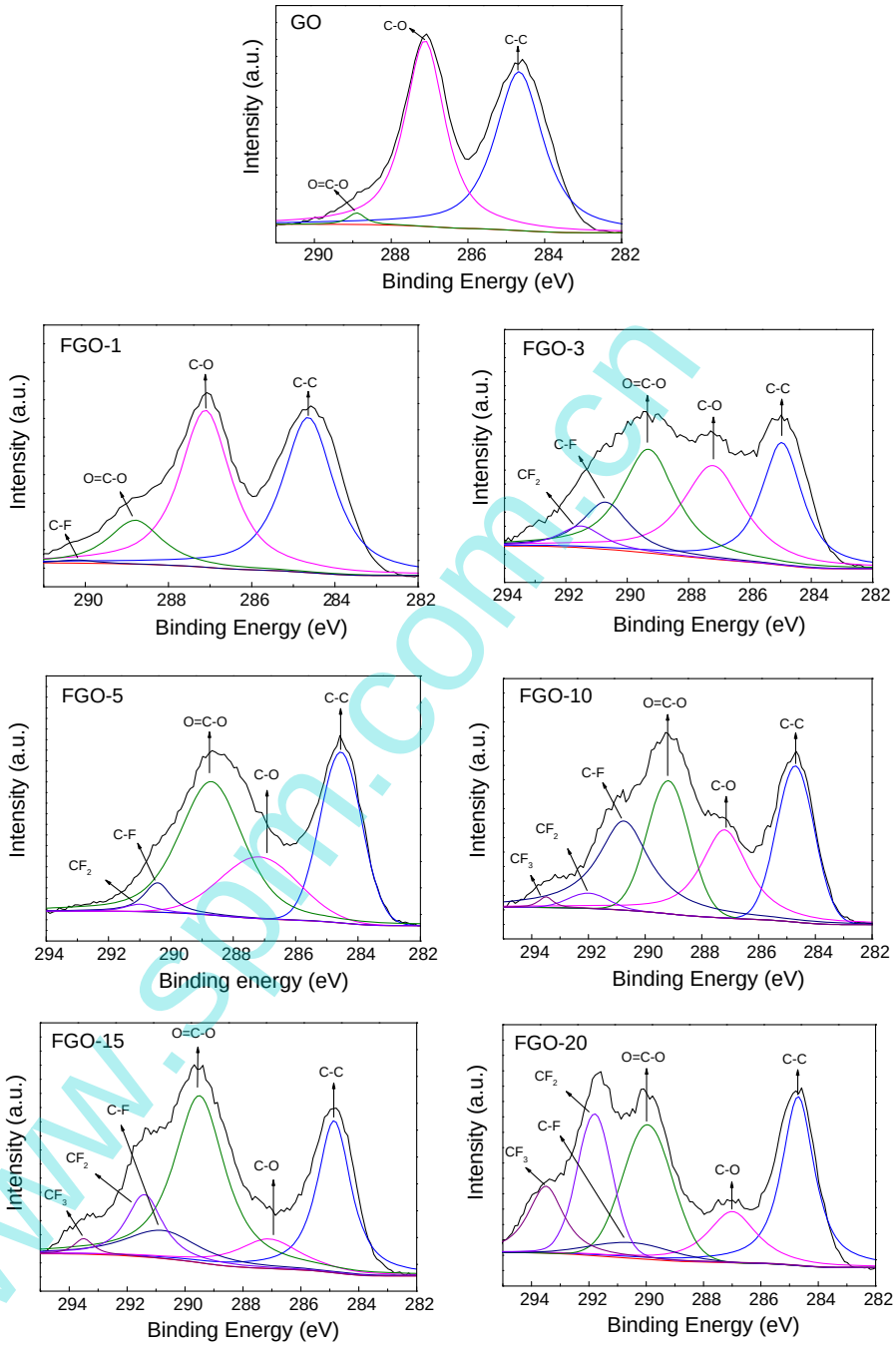

Fig. 3 Curve-fitting and raw curve of XPS C1s spectra of fluorinated and pristine GO

fluorination was in the form of an increasing of C–F, CF_2, and CF_3 covalent bond.

The hydrogen atoms bonding on the organic macromolecules (C–H and O–H) were easily substituted by fluorine atoms, and product HF was able to catalyze the fluorination of carbon materials. Catalysis of HF could probably contribute to the appearance of C–F bonds (Sato et al. 2008). The C–C bonds in aromatic region were progressively broken. These bands (in Fig. 3; Table 1) have been decreased with the increase of fluorination level, indicating that the aromatic regions were gradually fluorinated. This can

Table 1 Location, ascription, and content of chemical groups in C1s spectra of fluorinated and pristine GO

Samples	Functional groups (%)					
	C–C 284.6–284.8 (eV)	C–O 287.2–287.5 (eV)	O=C–O 288.5–288.9 (eV)	C–F 290.3–290.7 (eV)	CF_2 291.5–292.5 (eV)	CF_3 293.5–294.5 (eV)
GO	50.06	46.60	3.34	0	0	0
FGO-1	43.31	43.51	12.58	0.60	0	0
FGO-3	27.05	30.34	34.74	5.62	2.25	0
FGO-5	25.87	29.25	28.86	11.28	4.74	0
FGO-10	23.61	23.11	22.55	27.40	2.45	0.88
FGO-15	23.56	11.28	42.31	10.20	11.15	1.50
FGO-20	23.53	10.58	28.32	6.63	19.02	11.92

be seen as the rate-limiting step of the whole fluorination process. The contents of oxygen in FGO decreased evidently. Actually, the oxygen content was mainly influenced by two factors: decomposed reduction of GO resulting in the elimination of oxygen-related groups, and the substitution of oxygen-related groups by fluorine atom. The increase of F content resulted in the position of F peak shifting from 686.7 to 690 eV (Fig. 1), implying the enhancing of C–F covalence. The appropriate percentage of C–F covalence was conducive to enhance the chemical stability of fluorinated carbon materials (Gong et al. 2014).

As a gas–solid reaction (Shen et al. 2012), diffusion of CF_4 seriously influenced fluorination degree of the final products. The diffusion was generally determined by reaction temperature and time which have strong effects on chemical composition and structure of the final FGO, mainly owing to the honeycomb structure of GO that resulted from freeze-drying. The large surface area and interlayer space of GO made it possible for molecular CF_4 having a good contact with GO sheets, which blunts the impact of reaction times.

UV–Vis spectra of the fluorinated and pristine GO

UV–Vis absorption measurement was carried out as a probe for exploring the electronic configuration of carbon nanomaterial. The typical optical absorption spectra of GO, FGO-1, FGO-3, FGO-5, FGO-10, and FGO-20 were recorded, and the results are shown in Fig. 4. The GO spectrum has the characteristic maximum at 200–300 nm region, which was consistent with the literature data (Chang et al. 2010). The peak that appeared at 230 nm in the UV–Vis spectrum of GO contributed to the degree of the remaining conjugation (π–π*transition),and the shoulder around 300 nm should be ascribed to the *n*–π*transition of carbonyl groups. The absorbance in the 270–350 nm regions was thought to be caused by the conjugated aromatic domains. After fluorination, the shoulder gradually lost intensity and their absorption in the whole spectral region (>350 nm) decreased with fluorine concentration in the process of fluorination, reflecting the increase of π-electron concentration and structural order resulted from the restoration of sp^2 carbon and possible rearrangement of atoms. The FGO-20 solution almost does not absorb in the 400–800 nm, and its absorbance in the 270–350 nm region was very weak. This indicated that the electronic conjugation within the GO sheets was destroyed by fluorination.

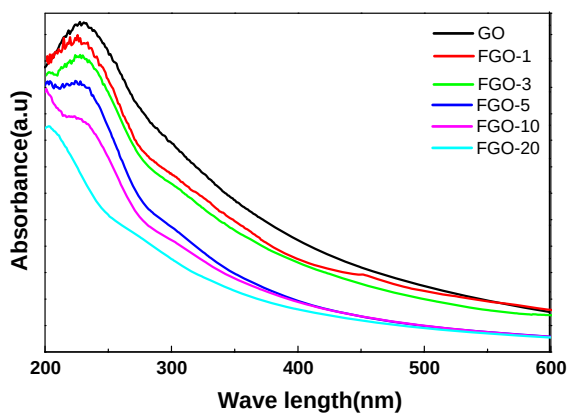

Fig. 4 UV–Vis spectra of the solution of GO and fluorinated GO

Morphologies of fluorinated and pristine GO

Figure 5a shows the SEM images of GO samples, and the honeycomb structures were formed from GO after freeze-drying, which has the large surface area and interlayer space. It is in favor of the reaction between GO and CF_4. And after the fluorinated functionalization, the color of GO has significantly changed (Fig. 5c). The digital photos were used to prove this phenomenon. As shown in Fig. 5b, c, the GO samples turned white after fluorination. Because of the honeycomb and porous structure of samples, GO has been treated uniformly in digital photos.

AFM and HRTEM observations were direct and convenient ways to explore the microstructure quality of graphene nanosheets. Prior to measurements, the graphene nanosheets were dispersed in ethanol by ultrasonication. This provides a facile approach to obtain mono-layered graphene for device fabrication or studies on the properties of individual sheets (Wang et al. 2012). A typical two-dimensional sheet-like structure is presented in Fig. 6e. Combining with the atomic ratio of F/O mentioned above (Fig. 2) and zeta potential values (Table 2), we took the typical samples (GO and FGO-10) to investigate the surface change of graphene samples. With plasma treatment for 10 min, a thinning effect was significantly obvious, according to the sample surface changes (Peltekis et al. 2012; Shen et al. 2012). As seen in Fig. 6b, d, the thickness of pristine GO is about 1.9 nm; however, the thickness of FGO-10 was declined to 1.3 nm after plasma treatment, which indicated that edge-defective nanostructure appeared on GO, and the partial oxygen-containing groups of GO samples were replaced by fluorine-containing groups. This result was also in good agreement with the above XPS characterization. The edge micrograph in Fig. 6e indicated that the FGO was of few layers, which was further confirmed by the HRTEM image (Fig. 6f). Meanwhile, as a result of fluorine and oxygen doping, the structure of FGO lost the perfect hexagonal structure of graphene and becomes more disordered (Gong et al. 2014). The disordered lattice was a reflection of a boat or chair structure configuration of sp^3-hybridized carbon, and this was also confirmed by high-resolution XPS spectra of C1s.

XRD patterns of fluorinated and pristine GO

Figure 7 shows the XRD patterns of GO and FGO-10 to reveal the influence of fluorination on the interlayer structure of GO. The characteristic peak of pristine GO around 10° can be clearly seen due to the incomplete exfoliation of graphite oxide. The relative intensity of pristine GO peak around 10° has been decreased, while the weak broad diffraction peak around 20–25° was strengthened after plasma treatment, indicating the reduction effect of plasma treatment and thus the decline in interlayer spacing of partial GO.

Dispersion behavior of fluorinated and pristine GO

To investigate the dispersion properties of FGO with different $R_{F/O}$, all samples were dissolved in distilled water and DMAc at 1 mg/ml by sonication for 1 h. Compared with the pristine GO, the FGO samples have a better dispersion in organic solution and a poor dispersion in water. The results from chemical analyses and morphological investigation proved that covalent C–F, CF_2, or CF_3 bonds have been grafted onto graphene, and unlike GO, owing to the invasion of hydrophobic fluorine and loss of hydrophilic

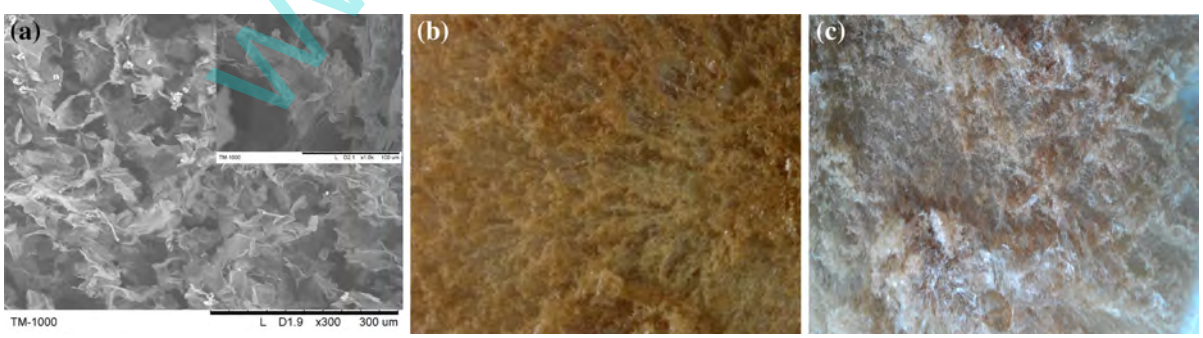

Fig. 5 **a** SEM images of GO samples after freeze-drying, digital photos of GO samples before (**b**) and after (**c**) fluorination

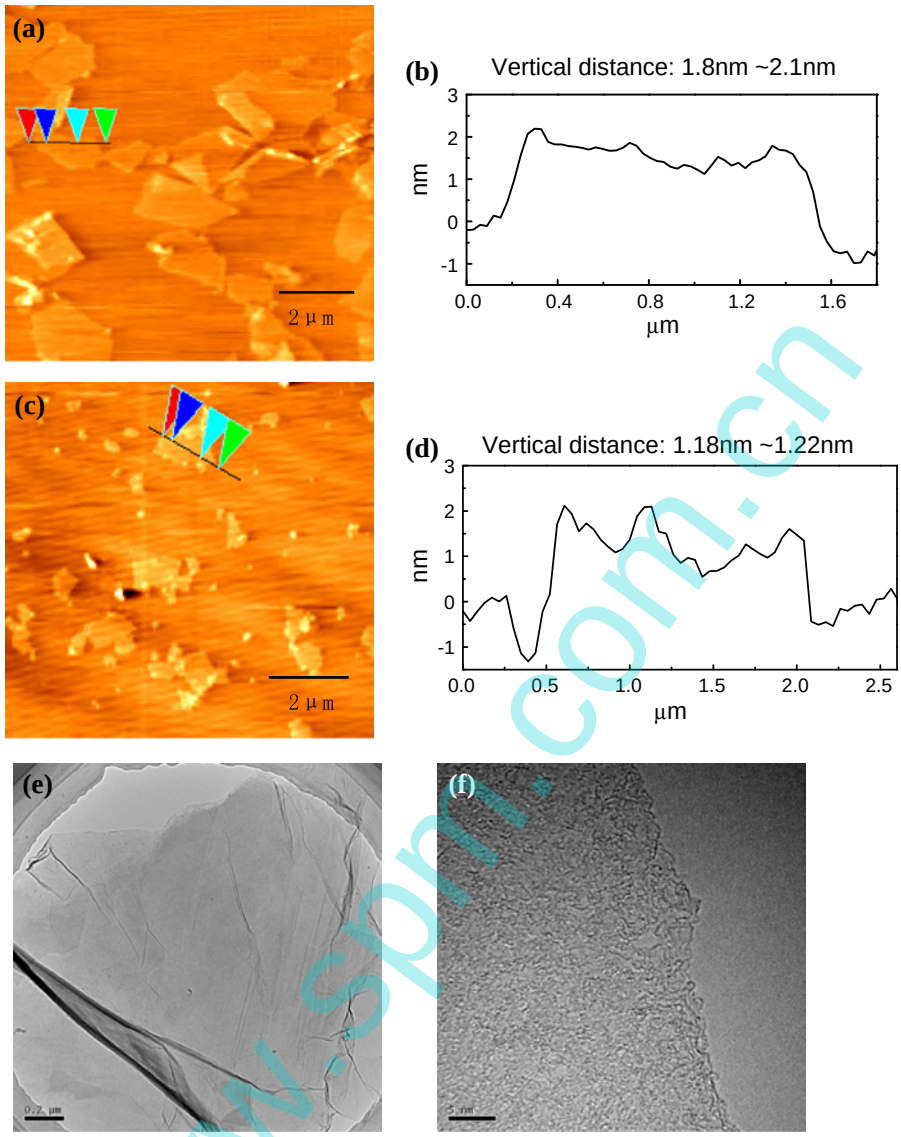

Fig. 6 Tapping mode AFM topographic images of **a** GO and **c** FGO-10, AFM cross-section of GO (**b**) and FGO-10 (**d**), and TEM (**e**) and HRTEM (**f**) micrographs of FGO-10

Table 2 Zeta potential values for GO and FGO solutions

Samples	Zeta potential in water (mV)	Zeta potential in DMAc (mV)
GO	−60.5 ± 0.65	−4.065 ± 0.5
FGO-1	−53.67 ± 0.8	−6.5 ± 0.53
FGO-3	−50.2 ± 0.7	−12.91 ± 0.49
FGO-5	−40.75 ± 0.85	−21.4 ± 0.62
FGO-10	−39.17 ± 0.7	−28.6 ± 0.58
FGO-15	−36.25 ± 0.63	−22.12 ± 0.7
FGO-20	−32.8 ± 0.72	−17.8 ± 0.59

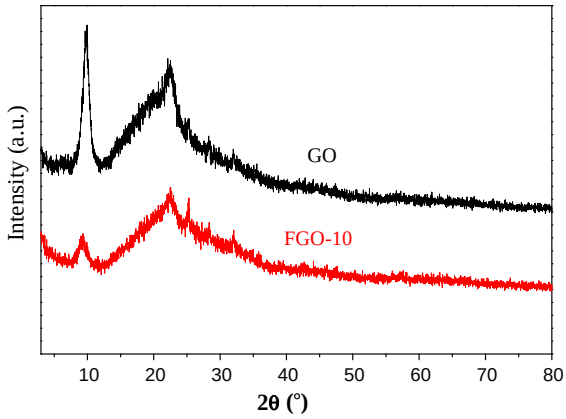

Fig. 7 XRD patterns of GO and FGO-10

oxygen atoms, the as-prepared FGO was difficult to be dispersed in water (Fig. 8; Table 2). When the solvent was replaced by DMAc, FGO can be dispersed effectively, especially FGO-10 and FGO-15. After sonication for 1 h, FGO dispersed well in organic solution and do not form aggregation at the bottom of bottle. This was consistent with the prevenient report (Gong et al. 2014). The improved dispersibility and stability of FGO samples can be ascribed to the enhanced conjugation between FGO and organic solvent. Interestingly, the dispersion of FGO in DMAc was not increased continuously with the increase in the time of plasma treatment.

Surface charge and colloidal stability of graphene in water and DMAc (1 mg/ml) were obtained by zeta potential measurements and visual evidence of settling (Male et al. 2012). It should be noted that the zeta potential confers the degree of repulsion between charged particles in dispersion, and a high zeta potential (negative or positive above 40 mV) was an indicator that the dispersion resists aggregation and consequently remains stable. Analysis of the zeta potential for the samples was negative in value (Table 2). For aqueous solutions, FGO had lower zeta potentials absolute value (−53.67 to −39.17 mV) than GO (−60.5 mV). In brief, GO with carboxyl, hydroxyl, and epoxy groups should result in more stable dispersions in water, compared with FGO with hydrophobic C–F, CF_2, and CF_3 groups. This hypothesis will be confirmed by the XPS spectra analysis. As can be found in Fig. 9a, the trend of C–O (hydroxyl/epoxy group) content became similar with the zeta potential of FGO in water, and the dispersion of FGO in water possibly resulted from the C–O content mainly.

But for organic solution, the zeta potentials of FGO was significantly more negative than GO. The zeta potential values of FGO-10 reached the lowest at −28.6 mV, as further fluorination degree, while the absolute values showed a slight decrease, indicating FGO-10 showed best dispersion and the $R_{F/O}$ was 1.35. According to the results in Tables 1 and 2, the zeta potential of FGO in DMAc was affected by C–F mainly, and it was shown that there was a linear variation of FGO zeta potential with the value of C–F content (Fig. 9b). The CF_2 and CF_3 contents were both increased after CF_4 plasma treatment.

Water contact angle of fluorinated and pristine GO film

Contact-angle measurements were widely used for the characterization of interaction potential between individual

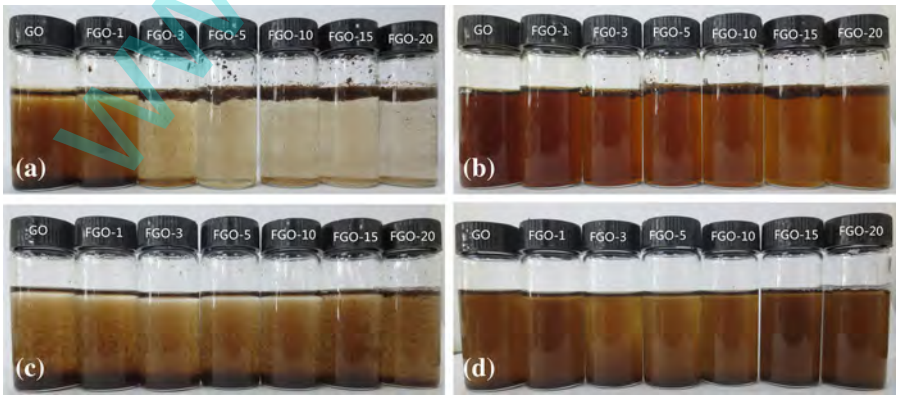

Fig. 8 Optical photographs of FGO dispersed in water (**a**) and DMAc (**c**) by shake and in water (**b**) and DMAc (**d**) by ultrasound

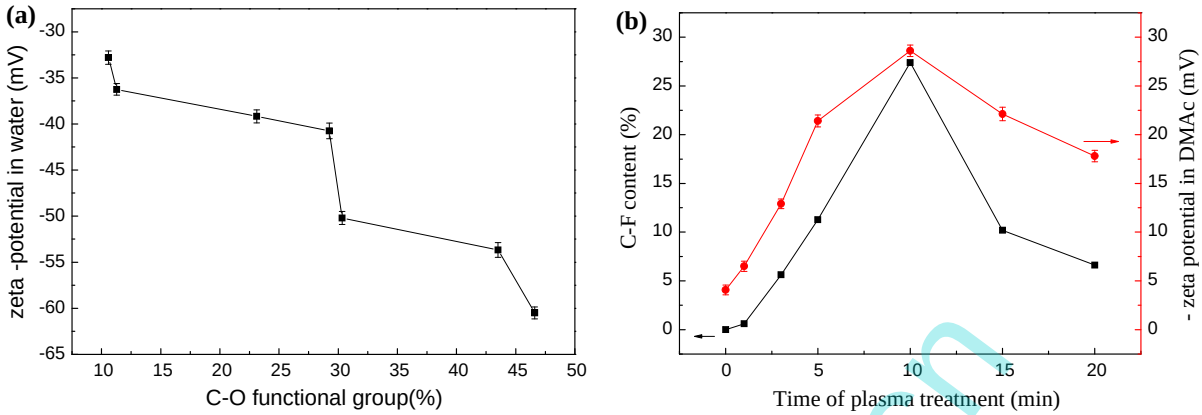

Fig. 9 Function of zeta potential in water (**a**) and DMAc (**b**) as C–O and C–F content

water molecule and graphene films surface (Taherian et al. 2013), and the results are shown in Fig. 10. And wetting property was one of the most important properties of graphene films, which could influence the dispersibility in water and organic solvents (Shanmugharaj et al. 2013). The pristine GO film had the lowest initial water contact angle of 62.2° and receding contact angle of 11° in Fig. 10, implying that the GO films were super-hydrophilic (Wei et al. 2014). Owing to the invasion of hydrophobic fluorine and loss of hydrophilic oxygen atoms after fluorination, the initial contact angles of FGO films gradually increased with the increasing treatment time, reflecting that the hydrophilic low-dimensional carbon nanomaterials were becoming hydrophobic. As for the FGO-15 and FGO-20, the graphene films were found to be neither hydrophilic nor hydrophobic. Furthermore, difference in the decaying rate of pristine GO film and FGO films showed obviously impeded water diffusing in 24 s determination. This was also confirmed by optical photographs of FGO dispersed in water and DMAc.

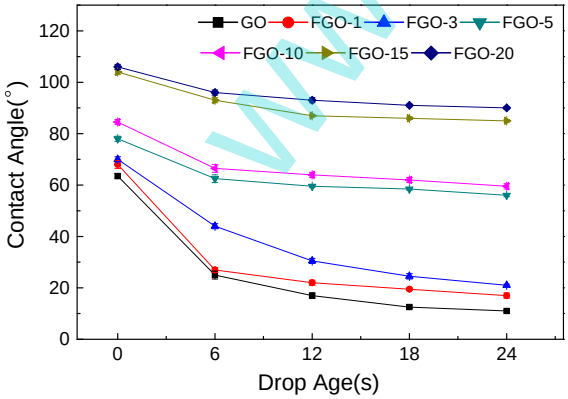

Fig. 10 Decay of water contact angle as a function of time

Conclusion

In conclusion, the work presents an easy, low-cost, and effective synthesis route of FGO by the plasma reaction between GO and CF_4. The results suggested that the fluorination degree could be easily controlled by varying the reaction time. Major findings from this study were as follows:

(a) Fluorine atoms have been attached to GO by CF_4 plasma, and the oxygen and carbon content decreased and the fluorine content increased with the increase in reaction time. C–F group was increased continuously in first 10 min and then decreased, which was different from the continuous increase of CF_2 and CF_3 groups.

(b) TEM and AFM results indicated that a thinning effect for GO was significantly obvious during the CF_4 plasma treatment and the as-synthesized FGO had small sheet size and was etched at the edge.

(c) The dispersion of FGO in water became weak with the increase in atomic ratio of F/O, which may be attributed to the decrease of C–O group. FGO-10 showed best dispersion at DMAc and it was found that there was a linear variation of FGO zeta potential with the value of C–F content, although FGO-20 possessed the most ratio of F/O, CF_2 group and CF_3 group.

(d) The film of GO was super-hydrophilic and there was a decrease in hydrophilicity of FGO film with the increase in plasma time. FGO-20 film was found to be neither hydrophilic nor hydrophobic.

Acknowledgments The work was funded by the National Natural Science Foundation of China (11175130) and the Petrochemical Joint Funds of National Natural Science Fund Committee-China National Petroleum Corporation (U1362108).

References

Ai W et al (2013) One-pot, aqueous-phase synthesis of graphene oxide functionalized with heterocyclic groups to give increased solubility in organic solvents. RSC Adv 3:45. doi:10.1039/c2ra22009a

Balandin AA, Ghosh S, Bao W, Calizo I, Teweldebrhan D, Miao F, Lau CN (2008) Superior thermal conductivity of single-layer graphene. Nano Lett 8:902–907. doi:10.1021/nl0731872

Bon SB, Valentini L, Verdejo R, Garcia Fierro JL, Peponi L, Lopez-Manchado MA, Kenny JM (2009) Plasma fluorination of chemically derived graphene sheets and subsequent modification with butylamine. Chem Mater 21:3433–3438. doi:10.1021/cm901039j

Bruna M, Massessi B, Battiato A, Vittone E, Borini S (2011) Synthesis and properties of monolayer graphene oxyfluoride. J Mater Chem 21:18730–18738

Chang H, Sun Z, Yuan Q, Ding F, Tao X, Yan F, Zheng Z (2010) Thin film field-effect phototransistors from bandgap-tunable, solution-processed, few-layer reduced graphene oxide films. Adv Mater 22:4872–4876

Chen M, Zhou H, Qiu C, Yang H, Yu F, Sun L (2012) Layer-dependent fluorination and doping of graphene via plasma treatment. Nanotechnology 23:115706. doi:10.1088/0957-4484/23/11/115706

Dreyer DR, Park S, Bielawski CW, Ruoff RS (2010) The chemistry of graphene oxide. Chem Soc Rev 39:228–240. doi:10.1039/b917103g

Eda G, Fanchini G, Chhowalla M (2008) Large-area ultrathin films of reduced graphene oxide as a transparent and flexible electronic material. Nat Nanotechnol 3:270–274

Geim AK, Novoselov KS (2007) The rise of graphene. Nat Mater 6:183

Gong P et al (2013) Photochemical synthesis of fluorinated graphene via a simultaneous fluorination and reduction route. RSC Adv 3:6327–6331

Gong P, Wang Z, Fan Z, Hong W, Yang Z, Wang J, Yang S (2014) Synthesis of chemically controllable and electrically tunable graphene films by simultaneously fluorinating and reducing graphene oxide. Carbon 72:176–184. doi:10.1016/j.carbon.2014.01.070

Lee C, Wei X, Kysar JW, Hone J (2008) Measurement of the elastic properties and intrinsic strength of monolayer graphene. Science 321:385–388. doi:10.1126/science.1157996

Loh KP, Bao Q, Ang P, Yang J (2010) The chemistry of graphene. J Mater Chem 20:2277–2289

Male KB, Lam E, Montes J, Luong JHT (2012) Noninvasive cell-based impedance spectroscopy for real-time probing inhibitory effects of graphene derivatives. ACS Appl Mater Interfaces 4:3643–3649. doi:10.1021/am301060z

Matsutani A, Tahara K, Iwasaki T, Hatano M (2013) Fluorination of graphene by reactive ion etching system using Ar/F_2 Plasma. Jpn J Appl Phys 52:06GD11. doi:10.7567/jjap.52.06gd11

Meyer JC, Geim AK, Katsnelson MI, Novoselov KS, Booth TJ, Roth S (2007) The structure of suspended graphene sheets. Nature 446:60–63

Nair RR et al (2010) Fluorographene: a two-dimensional counterpart of Teflon. Small 6:2877–2884

Novoselov KS, Geim AK, Morozov SV, Jiang D (2004) Electric field effect in atomically thin carbon films. Science 306:666–669

Palin DE, Wadsworth KD (1948) Structure of carbon monofluoride. Nature 162:925–926

Peltekis N, Kumar S, McEvoy N, Lee K, Weidlich A, Duesberg GS (2012) The effect of downstream plasma treatments on graphene surfaces. Carbon 50:395–403. doi:10.1016/j.carbon.2011.08.052

Plank NOV, Jiang LD, Cheung R (2003) Fluorination of carbon nanotubes in CF_4 plasma. Appl Phys Lett 83:2426–2428. doi:10.1063/1.1611621

Romero-Aburto R et al (2013) Fluorinated graphene oxide; a new multimodal material for biological applications. Adv Mater 25:5632–5637

Sato Y et al (2008) In vivo rat subcutaneous tissue response of binder-free multi-walled carbon nanotube blocks cross-linked by de-fluorination. Carbon 46:1927–1934. doi:10.1016/j.carbon.2008.08.003

Shanmugharaj AM, Yoon JH, Yang WJ, Ryu SH (2013) Synthesis, characterization, and surface wettability properties of amine functionalized graphene oxide films with varying amine chain lengths. J Colloid Interface Sci 401:148–154. doi:10.1016/j.jcis.2013.02.054

Shen C, Huang G, Cheng Y, Cao R, Ding F, Schwingenschlogl U, Mei Y (2012) Thinning and functionalization of few-layer graphene sheets by CF_4 plasma treatment. Nanoscale Res Lett 7:268–275. doi:10.1186/1556-276x-7-268

Shi C et al (2012) Monitoring influence of chemical preparation procedure on the structure of graphene nanosheets. Physica E 44:1420–1424. doi:10.1016/j.physe.2012.03.004

Si Y, Samulski ET (2008) Synthesis of water soluble graphene. Nano Lett 8:1679–1682

Stankovich S et al (2006) Graphene-based composite materials. Nature 442:282–286. doi:10.1038/nature04969

Stine R, Lee W-K, Whitener KEJ, Robinson JT, Sheehan PE (2013) Chemical stability of graphene fluoride produced by exposure to XeF_2. Nano Lett 13:4311–4316. doi:10.1021/nl4021039

Taherian F, Marcon V, van der Vegt NFA (2013) What is the contact angle of water on graphene? Langmuir 29:1457–1465. doi:10.1021/la304645w

Wang Z et al (2012) Synthesis of fluorinated graphene with tunable degree of fluorination. Carbon 50:5403–5410. doi:10.1016/j.carbon.2012.07.026

Wang X et al (2013) High-yield production of highly fluorinated graphene by direct heating fluorination of graphene-oxide. ACS Appl Mater Interfaces 5:8294–8299. doi:10.1021/am402958p

Wei N, Lv C, Xu Z (2014) Wetting of graphene oxide: a molecular dynamics study. Langmuir 30:3572–3578. doi:10.1021/la500513x

Wu X et al (2010) Preparation of aligned porous gelatin scaffolds by unidirectional freeze-drying method. Acta Biomater 6:1167–1177. doi:10.1016/j.actbio.2009.08.041

Xu T, Yang J, Liu J, Fu Q (2007) CF_4 plasma-induced grafting of fluoropolymer onto multi-walled carbon nanotube

powder. Appl Phys A 90:431–435. doi:10.1007/s00339-007-4295-z

Yue M et al (2015) Switchable hydrophobic/hydrophilic surface of electrospun poly(L-lactide) membranes obtained by CF_4 microwave plasma treatment. Appl Surf Sci 327:93–99. doi:10.1016/j.apsusc.2014.11.149

Zbořil R et al (2010) Graphene fluoride: a stable stoichiometric graphene derivative and its chemical conversion to graphene. Small 6:2885–2891

Zhang Y, Tan Y, Stormer HL, Kim P (2005) Experimental observation of the quantum Hall effect and Berry's phase in graphene. Nature 438:201–204. doi:10.1038/nature04235

Zhang M, Ma Y, Zhu Y, Che J, Xiao Y (2013) Two-dimensional transparent hydrophobic coating based on liquid-phase exfoliated graphene fluoride. Carbon 63:149–156. doi:10.1016/j.carbon.2013.06.066